Neuron, Vol. 40, 685–694, November 13, 2003, Copyright ©2003 by Cell Press

A Rapid Cellular FRET Assay of Polyglutamine Aggregation Identifies a Novel Inhibitor

Neurotechnique

Sonia K. Pollitt,[1] Judit Pallos,[2] Jieya Shao,[5] Urvee A. Desai,[5] Aye Aye K. Ma,[5] Leslie Michels Thompson,[3,4] J. Lawrence Marsh,[2] and Marc I. Diamond[5,*]

[1]Genentech, Inc.
South San Francisco, California 94080
[2]Department of Developmental and Cell Biology
[3]Department of Psychiatry and Human Behavior
[4]Department of Biological Chemistry
University of California, Irvine
Irvine, California 92697
[5]Department of Neurology
University of California, San Francisco
San Francisco, California 94143

Summary

Many neurodegenerative diseases, including tauopathies, Parkinson's disease, amyotrophic lateral sclerosis, and the polyglutamine diseases, are characterized by intracellular aggregation of pathogenic proteins. It is difficult to study modifiers of this process in intact cells in a high-throughput and quantitative manner, although this could facilitate molecular insights into disease pathogenesis. Here we introduce a high-throughput assay to measure intracellular polyglutamine protein aggregation using fluorescence resonance energy transfer (FRET). We screened over 2800 biologically active small molecules for inhibitory activity and have characterized one lead compound in detail. Y-27632, an inhibitor of the Rho-associated kinase p160ROCK, diminished polyglutamine protein aggregation ($EC_{50} \approx 5$ μM) and reduced neurodegeneration in a *Drosophila* model of polyglutamine disease. This establishes a novel high-throughput approach to study protein misfolding and aggregation associated with neurodegenerative diseases and implicates a signaling pathway of previously unrecognized importance in polyglutamine protein processing.

Introduction

Human neurodegenerative disorders such as the tauopathies (including Alzheimer's disease), Parkinson's disease, amyotrophic lateral sclerosis, and polyglutamine expansion diseases are all characterized by misfolding and intracellular aggregation of pathogenic proteins. These phenomena appear closely linked to pathology, although it remains uncertain whether they represent a step in pathogenesis or even a protective mechanism. It is clear, however, that polyglutamine misfolding and aggregation occurs in a controlled fashion: it is noted primarily in affected neurons in patients and is subject to regulation within the cell by various pathways (Chen et al., 2003; Diamond et al., 2000; Emamian et al., 2003; Humbert et al., 2002; Meriin et al., 2001; Wyttenbach et al., 2000). The cellular pathways and molecular mechanisms that regulate intracellular protein misfolding and aggregation in polyglutamine and other neurodegenerative diseases remain largely unknown but might ultimately be targeted to prevent neurodegeneration. Currently there are no facile, high-throughput methods with which to identify these pathways in mammalian cells.

A variety of high-throughput approaches have been applied to identify direct inhibitors of polyglutamine aggregation in vitro (Berthelier et al., 2001; Georgalis et al., 1998; Wanker et al., 1999). In these cases, formation of insoluble aggregates of purified peptides serves as a readout. However, these methods cannot uncover underlying mechanisms that regulate intracellular protein misfolding. In cultured cells, two basic approaches have been used to quantify aggregation: microscopy and detergent insolubility. However, such methods are quite labor intensive, can be prone to experimenter bias, and are not highly quantitative. Recently Kim et al. used fluorescence resonance energy transfer (FRET) combined with single-cell imaging to study the constituents of large macromolecular aggregates in cultured cells (Kim et al., 2002). This method, while providing relatively precise spatial resolution, is quite time and labor intensive and does not quantify the degree of polyglutamine protein aggregation within a population of cells. Moreover, by focusing only on large inclusions, this and other microscopy-based approaches ignore small oligomeric microaggregates that may play an important role in pathogenesis (Taylor et al., 2003). To overcome the limitations of current technology, we have developed a high-throughput assay based on FRET that allows quantitative measurement of polyglutamine protein aggregation within cultured cell monolayers and provides a novel approach to study the cell biology of polyglutamine expansion diseases.

Polyglutamine diseases derive from CAG-codon expansion in certain genes. This enlarges a tract of glutamines in the target protein that produces neurodegeneration when it exceeds a critical threshold. Spinobulbar muscular atrophy (SBMA) is a progressive motor neuron disease caused by polyglutamine expansion in the N terminus of the androgen receptor (AR) (Kennedy et al., 1968; La Spada et al., 1991); Huntington's disease (HD) is a progressive neuropsychiatric degenerative condition with an associated movement disorder and derives from a similar expansion in a protein of unknown function, huntingtin (htt) (Huntington Collaborative, 1993). Cellular toxicity in most diseases correlates with nuclear accumulation and inclusion formation of mutant protein and, in certain cases, may derive from "toxic fragments" produced through proteolysis (DiFiglia et al., 1997; Ellerby et al., 1999; Hodgson et al., 1999; Li et al., 1998; Merry et al., 1998).

Several lines of evidence suggest that cells form inclusions as a physiological response to pathogenic proteins, although it remains unclear whether this is a protective or harmful process. Neurons of the central nervous system predominantly form nuclear inclusions, especially in affected regions, whereas somatic tissues

*Correspondence: marcd@itsa.ucsf.edu

generally do not (DiFiglia et al., 1997; Li et al., 1998; Paulson et al., 1997). Activation of stress pathways via heat shock or JNK activation increases polyglutamine protein aggregation (Cowan et al., 2003; Meriin et al., 2001; Wyttenbach et al., 2000). In response to activation of Akt kinase, one group has reported decreased htt toxicity and aggregation in cell models (Humbert et al., 2002), while others report increased ataxin-1 toxicity and aggregation (Chen et al., 2003). Several reports indicate that cytoplasmic inclusion formation within cells is a microtubule-dependent process (Garcia-Mata et al., 1999; Muchowski et al., 2002; Taylor et al., 2003). Last, our prior work has demonstrated that overexpressed wild-type glucocorticoid receptor (GR) diminishes polyglutamine protein aggregation after activation by hormone agonist, whereas a mutant form (GRΔ) increases nuclear inclusion formation and polyglutamine-dependent toxicity (Diamond et al., 2000; Welch and Diamond, 2001). Thus, polyglutamine protein conversion from a soluble to an aggregated form appears to be a highly regulated process within the cellular milieu and is not driven simply by a propensity for self-association. To identify mechanisms that would not have been clearly predicted from prior knowledge, we chose to investigate the cellular regulation of aggregate formation using a high-throughput approach. Here we describe the development of this method, its use as a screening tool to identify a potential therapeutic compound, and new insights into a pathway that can regulate polyglutamine aggregation.

Results

Aggregated Polyglutamine Proteins Produce FRET when Fused to Fluorescent Proteins

To develop a screening assay, we began with an amino-terminal 127 amino acid fragment of AR containing either 25 glutamine repeats (ARN127(25)) or a pathologic expanded tract of 65 repeats (ARN127(65)). These polypeptides were fused at their carboxyl termini either to CFP or YFP coding sequences (Figure 1A). Similar truncated AR gene products have previously been shown to reproduce a neurodegenerative phenotype in transgenic animals and cell models (Abel et al., 2001; Merry et al., 1998; Welch and Diamond, 2001). When expressed transiently in mammalian cells, the unexpanded forms of the protein (ARN127(25)CFP/YFP) remained diffusely distributed throughout the cytoplasm (data not shown). In contrast, the expanded proteins (ARN127(65)CFP/YFP) spontaneously formed perinuclear or nuclear aggregates (Figure 1).

We measured FRET initially in transfected nonneural and neural cells by two distinct microscopy-based methods. First, photobleaching was used to test whether aggregate-containing cells could be distinguished from those with soluble protein based on differences in their FRET signals. When FRET occurs, photobleaching the acceptor (YFP) molecule increases donor (CFP) emission. For ease in imaging, we transfected COS-7 cells with ARN127(65)CFP/YFP and GRΔ to create a population of cells with diffuse protein or either cytoplasmic or nuclear aggregates. We examined individual cells under a microscope and quantified CFP emission before and after photobleaching YFP, using digital photography to record fluorescence intensities. Photobleaching increased CFP emission from either cytoplasmic or nuclear inclusions an average of ~20% but not from diffusely distributed protein (Figures 1G–1L). In cells expressing unexpanded protein there was no aggregation, and no FRET signal was detected. We also obtained similar results in HEK293 cells (data not shown). To confirm that polyglutamine aggregates would produce FRET in neural cells, we employed differentiated C17-2 neural precursor cells (Figures 1C–1F; Snyder et al., 1992). In this case, we measured FRET according to a three filter-set method, which corrects for CFP bleedthrough into the YFP emission spectrum and crossover activation of YFP by CFP excitation (Schaufele et al., 2003; Weatherman et al., 2002). We measured FRET in cells with nuclear aggregates versus those with diffuse distribution of protein. Whereas diffusely distributed protein produced no significant FRET signal (FRET/CFP = 0.023 ± .041, n = 8), nuclear aggregates had clear FRET signal (FRET/CFP = 0.176 ± .78, n = 19). Thus, by separate methods in neural and nonneural cells, both nuclear and cytoplasmic inclusions produced strong FRET, whereas diffusely distributed protein did not.

Detection of FRET Signal in Cell Monolayers Using Emission Scans in a Fluorescence Plate Reader

To monitor polyglutamine protein aggregation based on FRET in transfected cell monolayers, we created an assay system using a monochrometer-based fluorescence plate reader (FPR). We used HEK293 cells for their ease of transfection and high protein expression levels and our ability to induce a high degree of nuclear aggregation. We performed emission scans using excitation at either 435 nm or 485 nm, and controls of CFP and YFP alone to calculate CFP bleedthrough into the YFP spectrum, and crossover activation of YFP by 435 nm excitation. These scans detected a robust FRET signal from cells expressing a positive control YFP-CFP fusion protein (Figure 2A). Co-expression of individual CFP and YFP proteins produced no FRET, despite their colocalization as assayed by fluorescence microscopy (data not shown). To characterize the system, we monitored changes in polyglutamine protein aggregation following dexamethasone (dex) activation of co-expressed GR or GRΔ, as described previously by us: GR reduces AR and htt aggregation, whereas GRΔ increases nuclear aggregate formation and cell toxicity (Figure 1B; Diamond et al., 2000; Welch and Diamond, 2001). We observed a highly specific and reproducible correlation between FRET signal and polyglutamine protein aggregation. Emission scans on the FPR demonstrated a small FRET signal for ARN127(25)CFP/YFP that was not significantly modulated by dex (Figure 2B). By contrast, ARN127(65)CFP/YFP produced relatively strong FRET signals that were modulated as expected upon activation of GR (to reduce aggregation) or GRΔ (to increase aggregation) (Figure 2C). These were approximately 10%–20% of the signal strength from the YFP-CFP fusion. The intensity of the FRET signal correlated well with measures of aggregate formation made by direct

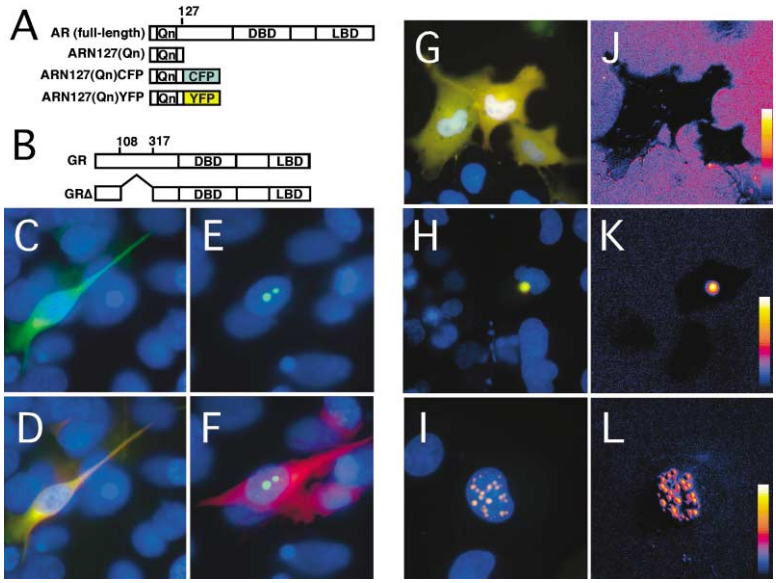

Figure 1. FRET Efficiencies of Soluble and Aggregated Forms of Fluorescently Labeled AR

(A and B) Diagrams of AR and GR constructs. (A) The full-length AR is shown for reference. Truncated forms contained the first 127 amino acids of AR (ARN127(Qn)) with either an unexpanded (n = 25) or expanded (n = 65) tract of glutamines. The truncated forms were fused to coding sequences of cyan and yellow fluorescent proteins (CFP and YFP, respectively). (B) Full-length GR and GRΔ, which carries a deletion of an activation domain, amino acids 108–317. The constitutive RSV promoter drove expression of each protein. DBD = DNA binding domain. LBD = ligand binding domain.

(C–F) Representative nuclear aggregates and diffuse distribution of ARN127(65)CFP/YFP in differentiated C17-2 neural cells used for measurement of FRET. Green signal represents polyglutamine protein; red represents a neuronal marker (neural tubulin) induced upon differentiation. Nuclei are counterstained with DAPI. Panels (C) and (D) show ARN127(65)CFP/YFP in diffuse distribution, with tubulin stain included in (D). Yellow color in (D) reflects superimposition of red and green signals. Panels (E) and (F) demonstrate nuclear aggregates, with tubulin stain included in (F). FRET was calculated in transfected cells using three filter-set measurements, with FRET/CFP ratios of .023 ± .041 (SD) for diffuse protein (n = 8), signifying no significant FRET, versus 0.176 ± 0.78 (SD) for nuclear aggregates (n = 19), signifying FRET.

(G–L) Images of diffuse and aggregated forms of AR and their qualitative FRET efficiencies in COS-7 cells. ARN127(65)CFP/YFP were coexpressed with GRΔ by transient transfection and cultured in the presence of 100 nM dex. Cells were fixed on coverslips and stained with DAPI. (G), (H), and (I) are standard fluorescence images taken on three channels (CFP, YFP, DAPI) and superimposed. Yellow results from colocalization of CFP and YFP. Images show the three characteristic polyglutamine protein distribution patterns: (G) diffuse, (H) cytoplasmic inclusion, and (I) nuclear inclusions. (J), (K), and (L) are calculated images that show the distribution of FRET efficiencies in the cells shown in (G), (H), and (I) based on applying the following formula to each pixel of the image: $(CFP_f - CFP_i)/CFP_f$, where CFP_i and CFP_f are the CFP intensities before and after photobleaching of YFP, respectively. The resulting calculated grayscale image was converted to color-scale using NIH-Image software. Note that diffuse protein had no significant increase in CFP signal following photobleaching, whereas both nuclear and perinuclear aggregates had increased CFP signal, indicating FRET.

observation with fluorescence microscopy (data not shown) and by detergent fractionation (Figure 2D).

Development of a High-Throughput FRET-Based Assay of Protein Aggregation

To create a high-throughput system, we replaced the two emission scans with three individual measurements using the following excitation/emission windows: CFP (435 nm ex/485 nm em), YFP (485 nm ex/530 nm em), and FRET (435 nm ex/530 nm em). This provided a quantitative measure of polyglutamine protein aggregation with no loss of fidelity (Figure 2E). Dose-response titrations of dex using either GR (to reduce aggregation) or GRΔ (to increase aggregation) demonstrated the accuracy of this system, allowing rederivation of the K_d of dex for GR and GRΔ (~1 nM) using FRET as a readout (Figure 2F). Thus, this detection method allows rapid and quantitative analysis of polyglutamine protein aggregation in a 96-well format. We confirmed the suitability of this system for high-throughput screening by calculating the Z value to be 0.67 according to the formula $1 - (3\sigma_x + 3\sigma_y)/|\mu_x - \mu_y|$, where σ_x and σ_y represent the standard deviation of positive and negative signals, respectively, and μ_x and μ_y represent the average value of the positive and negative signals, respectively (Zhang et al., 2000). This number reflects the ability of a screen to distinguish two distinct signals, taking into consideration the mean value and standard deviation of each (in this case aggregated versus nonaggregated polyglutamine protein); values >0.5 represent a highly robust system.

High-Throughput Screening for Inhibitors of Polyglutamine Aggregation

Prior to embarking on a large-scale screen, we began by testing a small number of well-characterized biologically active small molecules chosen on the basis of potential effects on polyglutamine protein aggregation and cell signaling. We cotransfected HEK293 cells with ARN127 (65)CFP/YFP and dex-activated GRΔ to maximize nuclear aggregate formation and cultured them in the presence of the compounds. FRET measurements were taken after 48 hr. To our surprise, one compound, Y-27632, decreased FRET by 40%, without concomitant loss of CFP or YFP signal (Figures 3A and 3B). Y-27632 is a well-characterized inhibitor of the Rho-activated serine/threonine kinase, p160ROCK (Ishizaki et al., 2000; Narumiya et al., 2000). A dose-response analysis demonstrated an EC_{50} of approximately 5 μM for the effect of Y-27632 on polyglutamine aggregation (Figure 3C). This is consistent with the EC_{50} of Y-27632 in modulation of stress-fiber formation via inhibition of p160ROCK (Ishizaki et al., 2000). Direct visualization (data not shown) and detergent fractionation confirmed our FPR findings (Figure 3D). Y-27632 also inhibited aggregation of htt exon 1-CFP and -YFP fusions containing 72 repeats

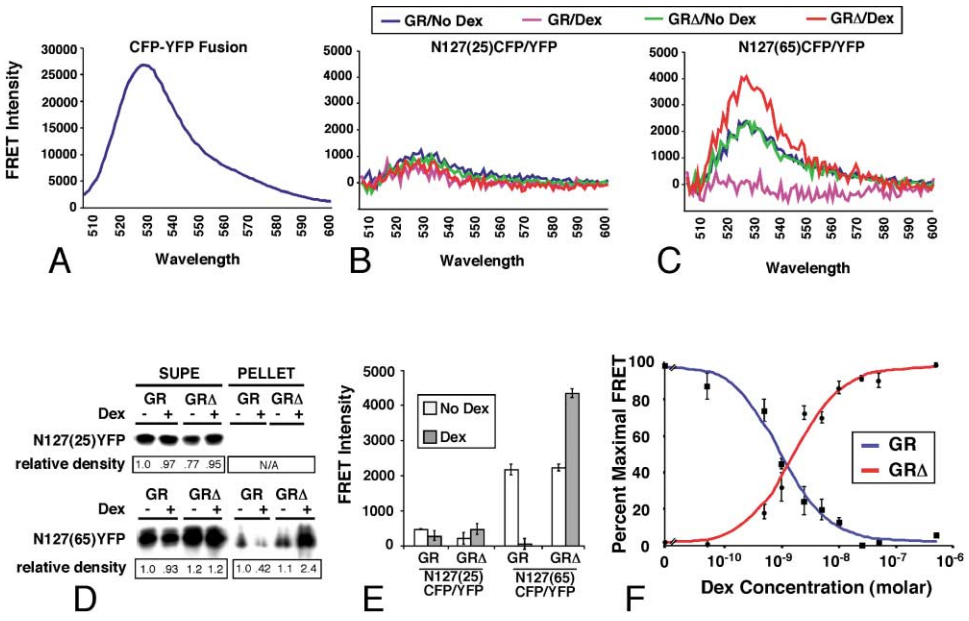

Figure 2. Detection of Polyglutamine Protein Aggregation in Cell Monolayers Using a Fluorescence Plate Reader

HEK293 cells were transfected with (A) YFP-CFP fusion, (B) ARN127(25)CFP/YFP plus GR or GRΔ, or (C) ARN127(65)CFP/YFP plus GR or GRΔ and cultured in a 96-well dish for 48 hr. GR and GRΔ mediate down- or upregulation, respectively, of polyglutamine protein aggregation when cultured with 100 nM dex.

(A–C) Emission peaks with maxima near 527 nm (YFP emission maximum) indicate FRET. (A) The YFP-CFP fusion produced a robust FRET signal. (B) The unexpanded AR127(25)CFP/YFP proteins produced a small FRET signal that was not significantly modulated by GR or GRΔ activation. (C) The expanded AR127(65)CFP/YFP proteins produced strong FRET signals in absence of dex (blue and green curves), which were diminished by activated GR (pink) and increased by activated GRΔ (red). Note the scale differences on the *y* axes.

(D) HEK293 cells were transfected with ARN127(25)YFP or ARN127(65)YFP along with GR or GRΔ. After culture for 48 hr with or without 100 nM dex, cells were lysed in 1% Triton/PBS. Following centrifugation at 15,000 × g, proportional amounts of SDS-denatured supernatant (SUPE) and pellet (PELLET) fractions were resolved by SDS-PAGE and immunoblotted with anti-AR antibody. Band intensities were determined by densitometry. AR127(25)YFP did not produce significant amounts of detergent-insoluble material. AR127(65)YFP expression resulted in significant amounts of detergent-insoluble material that was decreased by GR and increased by GRΔ following addition of dex.

(E) The same wells from (B) and (C) analyzed using excitation/emission windows on the FPR quantitatively reflect results from the emission scans. Error bars represent SEM.

(F) The K_d of dex for GR and GRΔ is accurately rederived via the FRET-based assay of aggregation. HEK293 cells were transfected with AR127(65)CFP/YFP and GR or GRΔ, and were treated with increasing amounts of dex. GR decreased and GRΔ increased FRET signals, with an EC_{50} of dex (1 nM) that reflects the known K_d of dex for GR. Curves were plotted as fractional signals with minimum signal arbitrarily set to zero and maximum set to 100.

(htt(72)CFP/YFP) (Figure 3B), demonstrating that its effects were not limited to a single polyglutamine protein.

Next, we tested this method as a high-throughput system by initiating a screen of 2800 biologically active compounds, comprising the Annotated Compound Library (ACL) (Root et al., 2003). This required small adaptations of our protocol to include internal controls and interassay standardization. Polyglutamine aggregation may be reduced by several means, including decreased protein expression, increased protein turnover, and molecular interactions within the cell that modify the propensity for misfolding. To control for the first two possibilities, we created an HEK293 cell line with stable expression of monomeric red fluorescent protein (mRFP), which allowed elimination of compounds that nonspecifically decreased steady-state protein levels. Likewise, to ensure accurate comparison of compounds across multiple experiments, we included on each plate a "no aggregation" control of unexpanded ARN127(25)CFP/YFP. For an individual experiment, each compound's activity was thus scaled between a 0% and 100% effect. Compounds were assayed in duplicate. We found that most had negligible effects on polyglutamine aggregation (0%–30% reduction), attributable primarily to well-well variation in the assay. In contrast, a small number of compounds showed more robust effects of >50% reduction in aggregation (Figure 3E). Detailed secondary screens will be required to characterize these hits; however, these results demonstrate the power of this screening method to identify inhibitors across a broad spectrum of compounds.

Genetic Analysis of Pathways Implicated by Y-27632

Although we identified a number of potential inhibitors from our large-scale screen, we chose to study further the effects of Y-27632. Thus, we tested whether a dominant-negative mutant of the putative target, p160ROCK(KD-IA), would also attenuate polyglutamine protein aggregation (Hirose et al., 1998; Ishizaki et al., 1997). Compared to empty expression vector, p160ROCK(KD-IA) decreased ARN127(65)CFP/YFP aggregation by ~20% (Figure 4A). While modest, these results were consistent with the pharmacologic effects of Y-27632 and raised

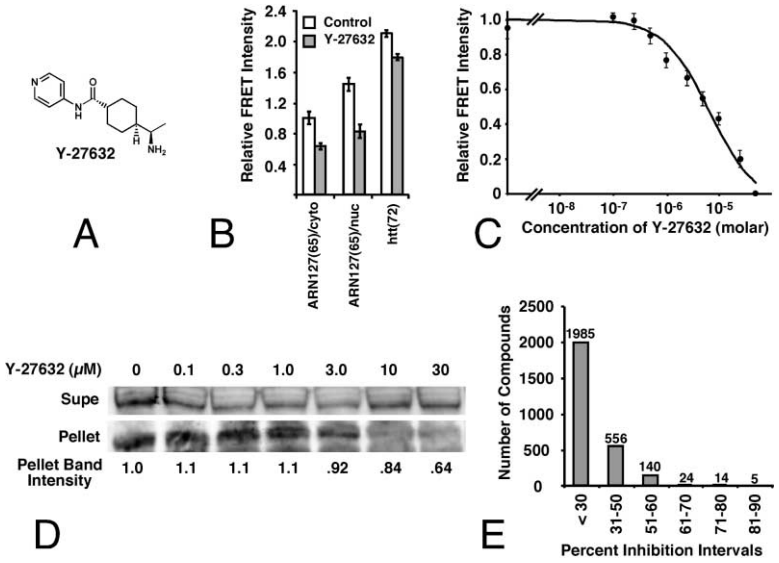

Figure 3. Y-27632, an Inhibitor of p160ROCK, Prevents Polyglutamine Protein Aggregation; Results of a High-Throughput Screen for Inhibitors of Aggregation

(A) Chemical structure of Y-27632.

(B) Y-27632 inhibits polyglutamine protein aggregation in the nucleus and cytoplasm. HEK293 cells were transfected with ARN127(65)CFP/YFP without and with GRΔ to produce cytoplasmic or nuclear inclusions, or htt(72)CFP/YFP alone, and cultured in the presence or absence of 50 μM Y-27632 for 48 hr. FRET intensity of ARN127(65)CFP/YFP in the absence of co-expressed GRΔ is set arbitrarily to 1. "Cyto" and "nuc" refer to the predominant location of inclusions in each condition (cytoplasmic versus nuclear). Error bars represent the SEM. All pair-wise analyses are significant to at least $p < .001$ by ANOVA.

(C) Y-27632 inhibited aggregation of ARN127(65)CFP/YFP with an EC_{50} of approximately 5 μM. Fractional FRET signals were plotted with minimum signal arbitrarily set to zero and maximum set to 100.

(D) Titration of Y-27632 with detergent fractionation confirmed the effect of Y-27632 on ARN127(65)CFP/YFP aggregation. HEK293 cells were transfected with ARN127(65)CFP/YFP and treated with the indicated amounts of Y-27632 for 48 hr. Detergent fractionation was followed by Western blot, which indicated that Y-27632 reduced ARN127(65)CFP/YFP detergent insolubility in a dose-dependent manner.

(E) Summary results from the Annotated Compound Library screen. The histogram reflects the total number of compounds in each activity range.

the possibility that p160ROCK signaling might be involved in polyglutamine aggregation.

p160ROCK is best known as an effector of RhoA but may also be controlled by other rho-GTPases, including Rac, to regulate cytoskeletal dynamics. In fact, in cells treated with Y-27632, we noticed cytoskeletal changes: cells extended longer processes and appeared to spread out farther on the culture dish (data not shown). To determine which GTPase might exert an effect on polyglutamine protein aggregation, we co-expressed constitutively active or dominant-negative mutants of RhoA, Rac1, and Cdc42 with ARN127(65)CFP/YFP and compared their effects to empty vector (pcDNA3). Dominant-positive and -negative RhoA and Cdc42 mutants each increased polyglutamine aggregation to varying degrees (data not shown). On the other hand, dominant-negative N17Rac1 suppressed aggregation ~20%, while its dominant-positive counterpart, V12Rac1, increased polyglutamine aggregation ~40% (Figure 4B). These experiments implicated the rho-GTPase family, and Rac1 in particular, as potential regulators of polyglutamine aggregation.

We further tested the role of Rac1 in this process by comparing two dominant-positive V12Rac1 mutants containing additional single amino acid substitutions in their effector loop domains. F37A selectively interferes with Rac1's interaction with p160ROCK, blocking regulation of lamellipodia formation while leaving intact its regulation of the JNK pathway. In contrast, Y40C has no effect on p160ROCK interaction but blocks JNK activation (Lamarche et al., 1996). The F37A mutation in V12Rac1 diminished its upregulation of aggregation, whereas the Y40C mutation did not (Figure 4B). Thus, Rac1 interaction with p160ROCK, or a structurally related protein, appears crucial to its regulation of polyglutamine aggregation. Taken together, this data leaves uncertain the precise mechanism by which Y-27632 functions but strongly implicates pathways that regulate the cytoskeleton in the control of polyglutamine aggregation.

Analysis of Y-27632 in a *Drosophila* Model of Neurodegeneration

Finally, we tested whether Y-27632 might have a therapeutic effect in a *Drosophila* model of polyglutamine neurodegenerative disease. In this model, a htt exon 1 fragment containing an expanded tract of 93 glutamines (htt exon1(Q93)) is expressed in all neurons under the control of the elav:Gal4 driver system. Photoreceptor neurons are easily observed as seven light-transmitting rhabdomeres within each ommatidium of the *Drosophila* compound eye. Expression of htt exon1 (Q93) causes progressive neurodegeneration of photoreceptor neurons, as demonstrated by reduction in the number of rhabdomeres present in each ommatidium (Steffan et al., 2001). Following eclosion, adult flies expressing the transgene were grown for 7 days in the presence or absence of 25 μM Y-27632 in their food. Drug treatment slowed the loss of photoreceptor neurons, as revealed by an increase in the average number of rhabdomeres per ommatidium, preventing 29% of the rhabdomere loss induced by polyglutamine protein overexpression (Figures 4C and 4D). Thus, in addition to reducing polyglutamine aggregation in mammalian cells, Y-27632 is neuroprotective in this *Drosophila* model of polyglutamine protein toxicity.

Discussion

In this work we have developed a quantitative, high-throughput FRET-based assay of polyglutamine aggregation in mammalian cell monolayers, demonstrated its

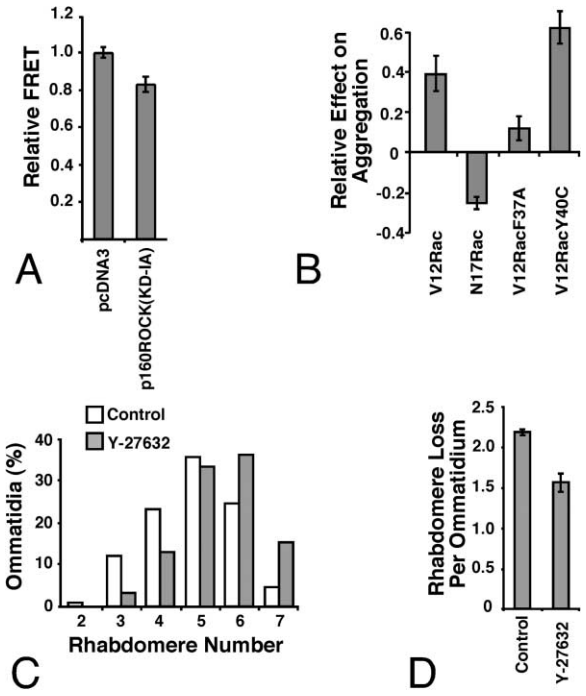

Figure 4. The Rac Pathway Regulates Polyglutamine Protein Aggregation; Y-27632 Functions in *Drosophila* to Reduce Polyglutamine-Dependent Neurodegeneration

(A and B) HEK293 cells were cotransfected with AR127(65)CFP/YFP and the indicated plasmids and assayed after 48 hr in culture. p160ROCK and Rac1 mutants were expressed from a pcDNA3 vector. Histograms show FRET values relative to cells cotransfected with AR127(65)CFP/YFP and empty vector (pcDNA3). (A) Co-expression of p160ROCK(KD-IA) reduced aggregation of AR127(65)CFP/YFP by ~20% ($p < .0001$ by ANOVA). (B) Overexpression of dominant-positive V12Rac increased aggregation, whereas overexpression of dominant-negative N17Rac decreased polyglutamine aggregation. Presence of the F37A mutation (which inhibits Rac1 binding to p160ROCK) reduced the activity of V12Rac, whereas the Y40C mutation (which does not affect Rac1 binding to p160ROCK) did not reduce V12Rac activity.

(C and D) Expanded polyglutamine htt exon 1(Q93) protein was expressed in *Drosophila* neurons, which results in loss of the normal number of seven visible rhabdomeres within each ommatidium. Adult flies were grown in the presence or absence of 25 μM Y-27632, and rhabdomeres were counted at seven days. (C) Y-27632 increased the percentage of ommatidia with six or seven rhabdomeres, with a corresponding decrease in the number of those with two, three, or four. (D) Analysis by average number of rhabdomeres/ommatidium per fly demonstrated a significant reduction in rhabdomere loss at 7 days, representing a 29% reduction in degeneration ($p < .0003$ by ANOVA).

utility as a high-throughput screening tool, and characterized in detail one lead compound. The use of FRET to study heterologous protein-protein interactions has been widely reported, even for polyglutamine proteins (Kim et al., 2002; Sekar and Periasamy, 2003). To our knowledge, however, this is the first use of such technology to study intracellular protein interactions on a quantitative, high-throughput basis, entirely distinct from microscopy. We demonstrated the ability of this approach to quantitatively and rapidly screen the ACL (approximately 2800 compounds) and are currently analyzing the candidates. In an initial screen, however, we examined a limited number of compounds and identified Y-27632 as an inhibitor of polyglutamine protein aggregation. We investigated the pathway implicated by Y-27632 and tested the efficacy of this compound in a *Drosophila* model of polyglutamine disease. Y-27632 is described as an inhibitor of the Rho-activated serine/threonine kinase p160ROCK, but like most kinase inhibitors, it can have off-target activities. We approximated its effect by overexpressing a dominant-negative p160ROCK mutant, p160ROCK(KD-IA). When we assayed potential upstream regulators of p160ROCK—RhoA, Rac1, and Cdc42—we found that a dominant-positive Rac1 mutant increased polyglutamine protein aggregation, whereas a dominant-negative mutant inhibited this process. Furthermore, a mutation in Rac1 that blocks its interaction with p160ROCK also reduced the effects of Rac1 on polyglutamine aggregation.

The interpretation of the effects of dominant-positive and -negative Rho, Rac, and Cdc42 mutants in this regulatory system is complex, however. There is significant cross-talk between these pathways, and one rho-GTPase may modulate the activity of another (Etienne-Manneville and Hall, 2002; Hirose et al., 1998). Although the effects of the Rac1 mutants do not present a clear mechanistic interpretation, together with Y-27632 they imply a significant role of the cytoskeleton in the regulation of aggregation. Based on imaging of the microtubule network in the presence and absence of Y-27632 (J.S., unpublished data), we believe that this mechanism is distinct from previously reported microtubule-dependent effects on aggregation (Johnston et al., 1998; Muchowski et al., 2002; Taylor et al., 2003). On the other hand, our results provide an alternative interpretation to the work of Peters et al., implying that arfaptin 2/POR1 (partner of Rac1) might regulate htt aggregation via influence on Rac1 signaling, rather than proteasome inhibition (Peters et al., 2002).

Several features of the current approach should be noted. By design it is not an assay of cell death or dysfunction and is limited to detection of modifiers of protein folding and aggregation. Secondary screens in *Drosophila* and cell models may be used determine whether candidate compounds have efficacy against cell dysfunction and death. In anticipation of possible arrayed cDNA library screens, which require high transfection efficiency and robust protein expression, the assay used here employed transfected nonneural cells (HEK293). Preliminary data from C17-2 neural cells, however, shows that polyglutamine aggregates may be detected via FRET, and in the future, use of stable neural cell lines expressing the CFP and YFP fusion proteins might increase detection of pathways relevant in vivo. Nonetheless, employing nonneural cells to study basic mechanisms associated with protein misfolding and aggregation, this assay identified a compound beneficial within the *Drosophila* nervous system.

Advantages of this approach are numerous. Because the assay depends on particular molecular events—misfolding and aggregation—it is likely that hits will be relatively specific to this process. In contrast to microscopy-based methods that rely on analysis of macromolecular aggregation, this FRET-based method in theory will produce signal even if aggregates consist of oligomeric structures that escape standard detection. Sec-

ond, because the assay is cell based, it has clear advantages over in vitro assays of protein aggregation, which are only capable of identifying direct modifiers of the protein of interest. Small molecules that directly target polyglutamine proteins will also score in this assay, but so will molecules such as Y-27632, which modulate misfolding and aggregation indirectly through action on regulatory pathways. We have comparatively little knowledge about the intracellular regulation of protein folding that underlies numerous neurodegenerative diseases. Although this method was applied here to polyglutamine proteins, it should also be amenable to study the regulation of folding of other aggregation-prone molecules responsible for neurodegenerative disease, such as tau, synuclein, superoxide dismutase, and prion protein.

Taken together, this work has contributed three elements to the study of polyglutamine disease. The FRET-based assay system offers a new approach to identify regulatory mechanisms that control protein misfolding and aggregation, possibly in multiple diseases. It complements existing strategies by creating opportunities to screen chemical and genetic libraries in a high-throughput format in the context of intact mammalian cells. This method might also be extended in the future to study libraries of arrayed cDNAs or siRNAs. Second, this work has identified regulatory pathways that implicate regulation of the cytoskeleton in the control of polyglutamine misfolding, aggregation, and toxicity. Last, the identification of Y-27632 as an inhibitor of polyglutamine protein aggregation in mammalian cells and of neurodegeneration in *Drosophila* may provide an important lead in the development of treatments for patients. Further study of the potential therapeutic value of Y-27632 and modulation of cytoskeletal regulatory pathways in fly, worm, and mouse models of polyglutamine disease should be very informative.

Experimental Procedures

Plasmid Construction

To construct ARN127-CFP and ARN127-YFP fusion proteins, coding sequences for ECFP and EYFP were PCR amplified from pECFP.C1 and pEYFP.C1 (Clontech) and were cloned downstream of ARN127 sequence into p6RARN127 (Diamond et al., 2000) to form p6RARN127(Qn)CFP or p6RARN127(Qn)YFP, with Q = 25 or 65 CAG repeats. To construct the YFP-CFP fusion protein, an intermediate vector was constructed in which the HincII/BsrGI fragment of pEYFP (Clontech) containing the coding region for YFP was placed into the Eco47III/BsrGI backbone of pEGFP-C1 (Clontech) to excise EGFP and create a vector with polylinkers on both 3′ and 5′ sides of the EYFP coding region. Then the BamHI fragment of this vector was subcloned into the BamHI/BglII backbone on ECFP-N3 to place EYFP in-frame and 5′ to ECFP. To construct htt exon 1-CFP and -YFP fusions, htt exon 1 fragment derived from plasmid qp72 (a gift from A. Kazantsev) was subcloned as a SalI/BamHI fragment, replacing the ARN127 coding sequence in p6RARN127CFP/YFP to form p6Rhtt(72)CFP and p6Rhtt(72)YFP. Plasmid encoding p160ROCK (KD-IA) was kindly provided by S. Narumiya. Plasmids encoding dominant-positive and -negative rho-GTPase mutants (RhoA, Rac1, Cdc42) were obtained from the cDNA Resource Center at the Guthrie Research Institute (http://www.guthrie.org). F37A and Y40C mutations in V12Rac were introduced by site-directed mutagenesis using QuickChange (Stratagene) and the following primers: F37A, GGA GAATATATCCCTACTGTCGCTGACAATTATTCTGCC (plus strand), GGCAGAATAATTGTCAGCGACAGTAGGGATATATTCTCC (minus strand); Y40C, GTCTTTGACAATTGTTCTGCCAATG (plus strand), CATTGGCAGAACAATTGTCAAAGAC (minus strand).

Cell Culture and Transfection

For photobleaching experiments, COS-7 cells were transfected on coverslips in 6-well dishes. Each well was transfected with 1 μg of a mixture of AR127(65)CFP/YFP and 1 μg GRΔ using 10 μl Plus and 12 μl Lipofectamine according to manufacturer's protocol (Invitrogen). After 5 hr, transfection medium was replaced with complete medium containing 100 nM dex, and cells were cultured for 48 hr to allow aggregate formation. For experiments in the fluorescence plate reader, high-throughput screening, and detergent fractionation, HEK293 cells in 6-well plates were transfected with a total of 2 μg of DNA using 10 μl Plus and 12 μl Lipofectamine according to manufacturer's protocol. To control for autofluorescence and light scattering by mammalian cells, a control group was transfected with 2 μg pcDNA3. To control for bleedthrough and crossover excitation, CFP and YFP controls were transfected with 1 μg pECFP-C1 (Clontech) and 1 μg pcDNA3 (Invitrogen) or 1 μg pEYFP-C1 (Clontech) and 1 μg pcDNA3, respectively. After 5 hr, cells were counted and plated into optically clear 96-well plates (Costar 3603) at a density of 60,000 cells/well. For assays of p160ROCK(KD-IA), it was necessary to reduce the amount of this plasmid by 80% due to toxicity at higher levels: 0.2 μg p160ROCK(KD-IA), 0.8 μg pcDNA3, and 1 μg of either 6RARN127(65)CFP/YFP or 6Rhtt(72)CFP/YFP were used. For assays of rho-GTPase mutants, 1 μg of each was used in conjunction with 1 μg of the polyglutamine expression plasmids. Transfections were performed in triplicate, and each experiment was repeated 6 times. C17-2 neural precursor cells were plated in 12-well plates and transfected using 4 μg of DNA and 4 μl of Lipofectamine 2000. 16 hr following transfection, cells were replated on coverslips coated with poly-L-lysine and laminin and grown in DME-H21 supplemented with 1% fetal bovine serum and 100 ng/ml each of NGF and mitomycin for 2 days. Polyglutamine protein was visualized by direct fluorescence; neuron-specific tubulin was visualized by immunostaining with mouse monoclonal antibody Neuro TUJ1 (Covance) at 1:1000.

Detection of FRET via Photobleaching of Fixed Cells

Fixed COS-7 cells on coverslips were mounted in 50% glycerol/PBS without bleach retardant 48 hr after transfection. All images were obtained using a 60× 1.4 N.A. lens (Olympus, Lake Success, NY) and N = 1.518 immersion oil. Digital images were acquired using a 12-bit cooled charge-coupled device on a multiwavelength wide-field optical sectioning microscopy system (Deltavision, Applied Precision, Issaquah, WA). Channels used for imaging were as follows: CFP: exciter D436/10, JP4 beamsplitter, emitter D470/30; YFP: exciter HQ500/14, JP4 beamsplitter, emitter HQ535/30 (Chroma Technology Corp., Brattleboro, VT). To create an image in which the intensity reflected an estimate of FRET efficiency, on a pixel-by-pixel basis the value of the initial CFP image was subtracted from the final CFP image obtained after photobleaching, and this difference was multiplied by 100 and divided by the final CFP image intensity: $100\times(CFP_{final} - CFP_{initial})/CFP_{final}$. Image arithmetic was performed using Deltavision software and converted from grayscale to color using NIH-Image 1.62 software.

Detection of FRET via Three Filter-Set Measurements

For FRET detection in C17-2 cells via three filter-set measurements, fixed cells on coverslips were analyzed by direct fluorescence microscopy. All images were collected using an Olympus 60× Plan Apochromat objective and quantitative fluorescence microscopy equipment as previously described (Schaufele et al., 2003; Weatherman et al., 2002). For each cell, three fluorescence channels were collected: the donor channel consisted of CFP excited with 431–440 nm light and CFP fluorescence collected at 455–485 nm, the acceptor channel consisted of YFP excited with 496–505 nm light and YFP fluorescence collected at 520–550 nm, and the FRET channel consisted of CFP excited with 431–440 nm light and YFP fluorescence collected at 520–550 nm. Cells separately expressing ARN127(65)CFP and ARN127(65)YFP were used to determine the separate contributions of the donor and acceptor fluorophores to each channel for both diffuse and aggregated protein.

Emission Scans on the Fluorescence Plate Reader

After 48 hr in culture, cells were fixed for 2 min in 10% formaldehyde/PBS, the formaldehyde was replaced with 200 μl per well of PBS,

and the cells were read on a fluorescence plate reader (SAFIRE, Tecan, Inc.). Automated scans were performed in which each well was excited at 435 ± 2.5 nm while monitoring emission from 455 ± 6 nm to 600 ± 6 nm (FRET scan) to record CFP and FRET signals and then excited at 485 ± 2.5 nm while monitoring emission from 500 ± 6 nm to 600 ± 6 nm (YFP scan) to record YFP signal. Data were analyzed as follows. First, the averaged signals from wells transfected with vector alone were used to background subtract all other signals. To normalize for CFP expression, a control sample transfected with CFP alone was used. Sample 435 nm and 485 nm emission curves were multiplied by the ratio of control CFP signal to sample CFP signal in the window 482–492 nm, following 435 nm excitation: $N_{CFP} = CFP_{control}/CFP_{sample}$. After such normalization, subtraction of the CFP control curve from the sample curve removes the contribution of CFP bleedthrough from the sample FRET scan. To adjust for YFP crossover activation, a control sample transfected with YFP alone was used. The control YFP control signal (em 520–530 nm) from 435 nm excitation was divided by the YFP control signal following 485 nm excitation to determine the following crossover activation ratio: $X_{YFP} = (YFP_{ex435/em520-530}/YFP_{ex485/em520-530})$. With this information, it is possible to subtract out the contribution of YFP crossover activation to the FRET signal. The resulting curve contains emission solely due to FRET: $FRET_{calc} = [N_{CFP} \times (Sample_{ex435})] - (CFP\ control_{ex435}) - [N_{CFP} \times (Sample_{ex485}) \times X_{YFP}]$.

FRET Measurements Using Fixed Excitation/Emission Windows

Automated measurements of each well were taken on the FPR using the following three windows: CFP ex 435 ± 2.5 nm/em 485 ± 6 nm; FRET ex 435 ± 2.5 nm/em 485 ± 6 nm; YFP ex 485 ± 2.5 nm/em 530 ± 6 nm. Data were analyzed as follows. All readings were background subtracted based on averaged readings from cells transfected with vector alone. Controls containing CFP alone were used to normalize sample readings in all three windows by the ratio of control-to-sample signal in the CFP window: $N_{CFP} = CFP_{control}/CFP_{sample}$. After this normalization, subtraction of CFP control signal in the FRET window from sample signal in the FRET window removes the contribution of CFP bleedthrough from the sample signal. Control samples containing YFP alone were used to characterize YFP crossover excitation as a percentage of signal in the YFP window that appeared the FRET window: $X_{YFP} = YFP_{FRET}/YFP_{YFP}$. Subtraction of this percentage of the sample signal in the YFP window from the sample signal in the FRET window removes the contribution of crossover excitation from the sample FRET signal. The remaining signal is due solely to FRET. $FRET_{calc} = (N_{CFP} \times Sample_{435/530}) - (Pure\ CFP_{435/530}) - [(N_{CFP} - (Sample_{485/530}) \times X_{YFP}]$.

Detergent Fractionation

To measure effects of GR and GRΔ, HEK293 cells were cultured in 3.5 cm wells and transfected with 1 μg of total DNA consisting of 0.5 μg of ARN127(Q25/65)YFP and 0.5 μg of p6RGR or p6RGRΔ. Cells were cultured in the presence or absence of 100 nM dexamethasone for 48 hr. For titration of Y-27632, cells were transfected with ARN127(65)CFP/YFP alone and cultured with the indicated amounts of drug. Cells were harvested by washing off the plate in PBS/5 mM EDTA, gentle centrifugation, and freezing of the pellets. Cell pellets were stored at −20°C until future use. At this time, ice-cold lysis buffer was prepared consisting of PBS with 1% Triton X-100 (Sigma) and 1 μg/ml each of aprotinin, leupeptin, and pepstatin (Sigma). Pellets were resuspended in 400 μl of lysis buffer, and lysis was performed by 10–15 passages through a 26 gauge needle to break up nuclei and shear chromatin. The lysate was centrifuged at 15,000 × g for 5 min at 4°C. 100 μl of the supernatant was removed and the remainder discarded. The pellet was then washed 1× with lysis buffer and again centrifuged at 15,000 × g. The pellet was then resuspended in 50 μl of SDS sample buffer and boiled for 10 min. Total protein was determined in each supernatant fraction according to the Bradford method, and fractions representing equivalent amounts of total protein were diluted into SDS sample buffer. Equivalent proportions of the pellet fractions were also diluted into SDS sample buffer, and samples were resolved by electrophoresis on a 10% polyacrylamide gel. After transfer to a nylon membrane, immunoblotting was performed using rabbit N-20 anti-AR antibody at 1:2000 dilution (Santa Cruz Biotechnology). Following secondary antibody incubation, blots were developed using chemiluminescent substrate and exposure to X-ray film. Densitometry scans were performed on the film using NIH Image 1.62 software. These experiments were repeated at least six times with similar results.

Limited Chemical Screen

HEK293 cells were transfected and replated in 96-well plates. Test wells were transfected with ARN127(65)CFP/YFP and GRΔ. Cells were cultured with 100 nM dex, which, in the context of GRΔ, produces predominantly nuclear aggregation. Test compounds were added to the culture medium in quadruplicate wells at the time of replating, and cells were assayed after 48 hr in culture. The following list of compounds was screened at the concentrations indicated, which were, where possible, approximately 2.5-, 5-, and 10-fold over the reported K_i or EC_{50} for each. Compound (major target: conc1; conc2; conc3), Chelerythrine (Protein Kinase C: 2 μM; 8 μM; 40 μM), KT5823 (Protein Kinase G: 0.5 μM; 10 μM; 2 μM), PD98659 (MEK: 5 μM; 19 μM; 95 μM), 4-Cyano-3-methyl-Isoquinoline (Protein Kinase A: 0.1 μM; 0.4 μM; 2 μM), KN62 (Cam Kinase II: 40 μM; 8 μM; 2 μM), Y-27632 (ROCK I & II: 0.5 μM; 2 μM; 10 μM), PP2 (Src Kinases: 0.013 μM; 0.05 μM; 0.25 μM), ZM336372 (C-RAF: 0.17 μM; 0.67 μM; 3.33 μM), SB202190 (P38 MAP Kinase: 0.75 μM; 3 μM; 15 μM), ML-9 (Myosin Light Chain Kinase: 0.01 μM; 0.04 μM; 0.2 μM), LY294002 (PI3 kinase: 5.0 μM; 20 μM; 100 μM), MG132 (Proteasome: 0.01 μM; 0.04 μM; 0.2 μM), TSA (Histone Deacetylase: 5 ng/ml), SAHA (Histone Deacetylase: 0.05 μM), Na-4-phenylbutyrate (Histone Deacetylase: 5 mM; 20 mM; 100 mM), Na-butyrate (Histone Deacetylase: 5 mM; 20 mM; 100 mM), and Geldanomycin (hsp90: 0.1 μg/ml; 0.4 μg/ml; 2 μg/ml).

High-Throughput Screen of the Annotated Compound Library

The ACL consisted of a collection of ~2800 biologically active small molecules (a gift from B. Stockwell). Daughter plates were created in duplicate containing the compounds at a concentration of 80 μg/ml from the stock 4 mg/ml 384-well microtiter plates using a Zymark SciClone ALH. Compounds were aliquoted in 96-well plates (Costar 3603) at a concentration of 4 μg/ml, at which most of the compounds are active but are not toxic to the cells. To screen the library, HEK293 cells stably expressing RFP were plated in 10 cm plates to obtain ~80% confluence on the day of transfection. Each plate was transfected with 2 μg of ARN127(65)CFP/YFP each, and 0.7 μg p6RGRΔ using 50 μl Plus reagent and 76 μl Lipofectamine according to manufacturer's protocol (Invitrogen). After 3 hr, complete medium was added and the plates were incubated further for 3 hr. Next, after adding 100 nM dex, the cells were counted and plated at a density of 70,000 cells/well in duplicate 96-well daughter plates containing single aliquots of compounds from the library. The cells were then cultured for ~48 hr to allow aggregate formation. After fixing the cells, FRET signal was measured according to methods described above. Several internal controls were used to standardize each experiment. Mock-transfected cells were used to control for background autofluorescence and light scattering. To control for CFP bleedthrough and crossover excitation of YFP, additional wells contained cells expressing ARN127(25)CFP or ARN127(25)YFP alone. RFP was measured to control for nonspecific effects on steady-state protein levels. ARN127(25)CFP/YFP expression served as a reference point for background FRET levels without aggregation (a theoretical maximum effect on aggregation inhibition). FRET measurements for each experiment were thus scaled between 100% (cells with no drug treatment) and 0% (FRET levels from unexpanded protein). Last, each plate also contained wells treated with Y-27632 (50 μM) as a positive control.

Assay of Y-27632 on Neurodegeneration in *Drosophila*

Transgenic flies were used, harboring a human huntingtin exon 1 fragment with 93 glutamines (htt exon 1(Q93)) that is expressed in all fly neurons under the control of the elav:Gal4 driver. Flies were treated by maintaining adults on food containing 25 μM Y-27632 or no drug supplement. Flies expressing the transgene display progressive degeneration of the photoreceptor neurons, which is revealed by a time-dependent decrease in the number of rhabdomeres

per ommatidium (Steffan et al., 2001). Normal fly eyes have seven visible rhabdomeres, while flies expressing htt exon1 (Q93) display reduced numbers of rhabdomeres. The number of rhabdomeres in treated versus untreated flies were analyzed 7 days posteclosion by the pseudopupil technique as described (Steffan et al., 2001). Approximately 50–60 ommatidia were analyzed for rhabdomere content on each of 10–12 flies from each treatment group, and the average number of rhabdomeres per ommatidium in each individual was determined. Percent rhabdomere loss was calculated as 100 × ((7 − average number remaining)/7) before and after treatment.

Acknowledgments

Fred Schaufele provided invaluable assistance performing FRET measurements in C17-2 cells. Brent Stockwell kindly provided the Annotated Compound Library. The authors also wish to thank the following individuals for critical review of the manuscript: Henry Bourne, Ivan Diamond, William Welch, Huda Zoghbi, Diane Merry, J. Paul Taylor, and George Jackson. Fei Wang kindly provided chemicals used in the limited chemical screen. This work was supported by a Cure HD Initiative of the Hereditary Disease Foundation (L.M.T. and J.L.M.), Coalition for the Cure of the Huntington's Disease Society of America (L.M.T.), NINDS award NS045283 (J.L.M.), NINDS award 1R21NS045350-01 (M.I.D.), the Muscular Dystrophy Association (M.I.D.), the Sandler Family Supporting Foundation (M.I.D.), and NIH Grant BM3355 (J.P.). This work was also made possible through access to the National *Drosophila* Stock Center in Bloomington, IN.

Received: June 2, 2003
Revised: September 10, 2003
Accepted: September 25, 2003
Published: November 12, 2003

References

Abel, A., Walcott, J., Woods, J., Duda, J., and Merry, D. (2001). Expression of expanded repeat androgen receptor produces neurologic disease in transgenic mice. Hum. Mol. Genet. *10*, 107–116.

Berthelier, V., Hamilton, J.B., Chen, S., and Wetzel, R. (2001). A microtiter plate assay for polyglutamine aggregate extension. Anal. Biochem. *295*, 227–236.

Chen, H.K., Fernandez-Funez, P., Acevedo, S.F., Lam, Y.C., Kaytor, M.D., Fernandez, M.H., Aitken, A., Skoulakis, E.M., Orr, H.T., Botas, J., and Zoghbi, H.Y. (2003). Interaction of Akt-phosphorylated ataxin-1 with 14–3-3 mediates neurodegeneration in spinocerebellar ataxia type 1. Cell *113*, 457–468.

Cowan, K.J., Diamond, M.I., and Welch, W.J. (2003). Polyglutamine protein aggregation and toxicity are linked to the cellular stress response. Hum. Mol. Genet. *12*, 1377–1391.

Diamond, M.I., Robinson, M.R., and Yamamoto, K.R. (2000). Regulation of expanded polyglutamine protein aggregation and nuclear localization by the glucocorticoid receptor. Proc. Natl. Acad. Sci. USA *97*, 657–661.

DiFiglia, M., Sapp, E., Chase, K.O., Davies, S.W., Bates, G.P., Vonsattel, J.P., and Aronin, N. (1997). Aggregation of huntingtin in neuronal intranuclear inclusions and dystrophic neurites in brain. Science *277*, 1990–1993.

Ellerby, L.M., Hackam, A.S., Propp, S.S., Ellerby, H.M., Rabizadeh, S., Cashman, N.R., Trifiro, M.A., Pinsky, L., Wellington, C.L., Salvesen, G.S., et al. (1999). Kennedy's disease: caspase cleavage of the androgen receptor is a crucial event in cytotoxicity. J. Neurochem. *72*, 185–195.

Emamian, E.S., Kaytor, M.D., Duvick, L.A., Zu, T., Tousey, S.K., Zoghbi, H.Y., Clark, H.B., and Orr, H.T. (2003). Serine 776 of ataxin-1 is critical for polyglutamine-induced disease in SCA1 transgenic mice. Neuron *38*, 375–387.

Etienne-Manneville, S., and Hall, A. (2002). Rho GTPases in cell biology. Nature *420*, 629–635.

Garcia-Mata, R., Bebok, Z., Sorscher, E.J., and Sztul, E.S. (1999). Characterization and dynamics of aggresome formation by a cytosolic GFP-chimera. J. Cell Biol. *146*, 1239–1254.

Georgalis, Y., Starikov, E.B., Hollenbach, B., Lurz, R., Scherzinger, E., Saenger, W., Lehrach, H., and Wanker, E.E. (1998). Huntingtin aggregation monitored by dynamic light scattering. Proc. Natl. Acad. Sci. USA *95*, 6118–6121.

Hirose, M., Ishizaki, T., Watanabe, N., Uehata, M., Kranenburg, O., Moolenaar, W.H., Matsumura, F., Maekawa, M., Bito, H., and Narumiya, S. (1998). Molecular dissection of the Rho-associated protein kinase (p160ROCK)-regulated neurite remodeling in neuroblastoma N1E–115 cells. J. Cell Biol. *141*, 1625–1636.

Hodgson, J.G., Agopyan, N., Gutekunst, C.A., Leavitt, B.R., LePiane, F., Singaraja, R., Smith, D.J., Bissada, N., McCutcheon, K., Nasir, J., et al. (1999). A YAC mouse model for Huntington's disease with full-length mutant huntingtin, cytoplasmic toxicity, and selective striatal neurodegeneration. Neuron *23*, 181–192.

Humbert, S., Bryson, E.A., Cordelieres, F.P., Connors, N.C., Datta, S.R., Finkbeiner, S., Greenberg, M.E., and Saudou, F. (2002). The IGF-1/Akt pathway is neuroprotective in Huntington's disease and involves Huntingtin phosphorylation by Akt. Dev. Cell *2*, 831–837.

Huntington Collaborative (The Huntington's Disease Collaborative Research Group). (1993). A novel gene containing a trinucleotide repeat that is expanded and unstable on Huntington's disease chromosomes. Cell *72*, 971–983.

Ishizaki, T., Naito, M., Fujisawa, K., Maekawa, M., Watanabe, N., Saito, Y., and Narumiya, S. (1997). p160ROCK, a Rho-associated coiled-coil forming protein kinase, works downstream of Rho and induces focal adhesions. FEBS Lett. *404*, 118–124.

Ishizaki, T., Uehata, M., Tamechika, I., Keel, J., Nonomura, K., Maekawa, M., and Narumiya, S. (2000). Pharmacological properties of Y-27632, a specific inhibitor of rho-associated kinases. Mol. Pharmacol. *57*, 976–983.

Johnston, J.A., Ward, C.L., and Kopito, R.R. (1998). Aggresomes: a cellular response to misfolded proteins. J. Cell Biol. *143*, 1883–1898.

Kennedy, W.R., Alter, M., and Sung, J.H. (1968). Progressive proximal spinal and bulbar muscular atrophy of late onset. A sex-linked recessive trait. Neurology *18*, 671–680.

Kim, S., Nollen, E.A., Kitagawa, K., Bindokas, V.P., and Morimoto, R.I. (2002). Polyglutamine protein aggregates are dynamic. Nat. Cell Biol. *4*, 826–831.

Lamarche, N., Tapon, N., Stowers, L., Burbelo, P.D., Aspenstrom, P., Bridges, T., Chant, J., and Hall, A. (1996). Rac and Cdc42 induce actin polymerization and G1 cell cycle progression independently of p65PAK and the JNK/SAPK MAP kinase cascade. Cell *87*, 519–529.

La Spada, A.R., Wilson, E.M., Lubahn, D.B., Harding, A.E., and Fischbeck, K.H. (1991). Androgen receptor gene mutations in X-linked spinal and bulbar muscular atrophy. Nature *352*, 77–79.

Li, M., Miwa, S., Kobayashi, Y., Merry, D.E., Yamamoto, M., Tanaka, F., Doyu, M., Hashizume, Y., Fischbeck, K.H., and Sobue, G. (1998). Nuclear inclusions of the androgen receptor protein in spinal and bulbar muscular atrophy. Ann. Neurol. *44*, 249–254.

Meriin, A.B., Mabuchi, K., Gabai, V.L., Yaglom, J.A., Kazantsev, A., and Sherman, M.Y. (2001). Intracellular aggregation of polypeptides with expanded polyglutamine domain is stimulated by stress-activated kinase MEKK1. J. Cell Biol. *153*, 851–864.

Merry, D.E., Kobayashi, Y., Bailey, C.K., Taye, A.A., and Fischbeck, K.H. (1998). Cleavage, aggregation and toxicity of the expanded androgen receptor in spinal and bulbar muscular atrophy. Hum. Mol. Genet. *7*, 693–701.

Muchowski, P.J., Ning, K., D'Souza-Schorey, C., and Fields, S. (2002). Requirement of an intact microtubule cytoskeleton for aggregation and inclusion body formation by a mutant huntingtin fragment. Proc. Natl. Acad. Sci. USA *99*, 727–732.

Narumiya, S., Ishizaki, T., and Uehata, M. (2000). Use and properties of ROCK-specific inhibitor Y-27632. Methods Enzymol. *325*, 273–284.

Paulson, H.L., Perez, M.K., Trottier, Y., Trojanowski, J.Q., Subramony, S.H., Das, S.S., Vig, P., Mandel, J.L., Fischbeck, K.H., and Pittman, R.N. (1997). Intranuclear inclusions of expanded polyglutamine protein in spinocerebellar ataxia type 3. Neuron *19*, 333–344.

Peters, P.J., Ning, K., Palacios, F., Boshans, R.L., Kazantsev, A.,

Thompson, L.M., Woodman, B., Bates, G.P., and D'Souza-Schorey, C. (2002). Arfaptin 2 regulates the aggregation of mutant huntingtin protein. Nat. Cell Biol. *4*, 240–245.

Root, D.E., Flaherty, S.P., Kelley, B.P., and Stockwell, B.R. (2003). Biological mechanism profiling using an annotated compound library. Chem. Biol. *10*, 881–892.

Schaufele, F., Wang, X., Liu, X., and Day, R.N. (2003). Conformation of CCAAT/enhancer-binding protein alpha dimers varies with intranuclear location in living cells. J. Biol. Chem. *278*, 10578–10587.

Sekar, R.B., and Periasamy, A. (2003). Fluorescence resonance energy transfer (FRET) microscopy imaging of live cell protein localizations. J. Cell Biol. *160*, 629–633.

Snyder, E.Y., Deitcher, D.L., Walsh, C., Arnold-Aldea, S., Hartwieg, E.A., and Cepko, C.L. (1992). Multipotent neural cell lines can engraft and participate in development of mouse cerebellum. Cell *68*, 33–51.

Steffan, J.S., Bodai, L., Pallos, J., Poelman, M., McCampbell, A., Apostol, B.L., Kazantsev, A., Schmidt, E., Zhu, Y.Z., Greenwald, M., et al. (2001). Histone deacetylase inhibitors arrest polyglutamine-dependent neurodegeneration in *Drosophila*. Nature *413*, 739–743.

Taylor, J.P., Tanaka, F., Robitschek, J., Sandoval, C.M., Taye, A., Markovic-Plese, S., and Fischbeck, K.H. (2003). Aggresomes protect cells by enhancing the degradation of toxic polyglutamine-containing protein. Hum. Mol. Genet. *12*, 749–757.

Wanker, E.E., Scherzinger, E., Heiser, V., Sittler, A., Eickhoff, H., and Lehrach, H. (1999). Membrane filter assay for detection of amyloid-like polyglutamine-containing protein aggregates. Methods Enzymol. *309*, 375–386.

Weatherman, R.V., Chang, C.Y., Clegg, N.J., Carroll, D.C., Day, R.N., Baxter, J.D., McDonnell, D.P., Scanlan, T.S., and Schaufele, F. (2002). Ligand-selective interactions of ER detected in living cells by fluorescence resonance energy transfer. Mol. Endocrinol. *16*, 487–496.

Welch, W.J., and Diamond, M.I. (2001). Glucocorticoid modulation of androgen receptor nuclear aggregation and cellular toxicity is associated with distinct forms of soluble expanded polyglutamine protein. Hum. Mol. Genet. *10*, 3063–3074.

Wyttenbach, A., Carmichael, J., Swartz, J., Furlong, R.A., Narain, Y., Rankin, J., and Rubinsztein, D.C. (2000). Effects of heat shock, heat shock protein 40 (HDJ-2), and proteasome inhibition on protein aggregation in cellular models of Huntington's disease. Proc. Natl. Acad. Sci. USA *97*, 2898–2903.

Zhang, J.H., Chung, T.D., and Oldenburg, K.R. (2000). Confirmation of primary active substances from high throughput screening of chemical and biological populations: a statistical approach and practical considerations. J. Comb. Chem. *2*, 258–265.